Multimodel Combination Bathymetry Inversion Approach Based on Geomorphic Segmentation in Coral Reef Habitats Using ICESat-2 and Multispectral Satellite Images

Xiuling Zuo, Juncan Teng, Fenzhen Su, Zhengxian Duan, and Kefu Yu

***Abstract*—Owing to the high spatial heterogeneity of substrate types and terrain, the present satellite-derived bathymetry (SDB) methods have low accuracy in deriving large-scale bathymetry in coral reef habitats. Taking 11 coral reefs of Xisha Islands (ocean area of 607 km^2) in the South China Sea as the study area, a parametric multimodel combination approach based on geomorphic segmentation (PMCGS) for obtaining bathymetry was constructed by combining the Ice, Cloud and Land Elevation Satellite-2 (ICESat-2) data with Gaofen-1 (GF-1) medium- and Worldview-2/3 (WV-2/3) high-resolution multispectral images. In this approach, five parametric SDB models were trained in each geomorphic zone by combining ICESat-2 and multispectral satellite images. Then, the optimal SDB models of each geomorphic zone were combined and extrapolated to other coral reefs in the same geomorphic zone. Results showed that the multiple ratios model was optimal for the reef flat, shallow lagoon, and patch reef zones. The binomial model was optimal for the reef slope and deep lagoon zones. Validated by the in situ bathymetric data and ICESat-2 data, the bathymetry inverted using the PMCGS had an RMSE of 0.91 m in GF-1 image and 0.70–0.88 m in WV-2/3 images when extrapolated to other reefs, which is significantly more accurate than active–passive one entire model methods with the same resolution. Our method performed better at 0–10 m and 15–25 m depth than the results obtained from previous studies, especially in the shallow water areas of the reef flat and shallow lagoon. The proposed PMCGS can efficiently improve the bathymetry inversion accuracy of medium- and high-resolution satellite images and it has great potential applications in deriving large-scale bathymetry, especially in Indo-Pacific coral reef habitats.**

***Index Terms*—Bathymetry, coral reef, geomorphology, Ice, Cloud and Land Elevation Satellite-2 (ICESat-2), multispectral image.**

Received 24 May 2024; revised 11 August 2024, 16 October 2024, and 9 December 2024; accepted 21 December 2024. Date of publication 26 December 2024; date of current version 15 January 2025. This work was supported in part by the National Natural Science Foundation of China under Grant 42276182 and Grant 42090041, in part by the Natural Science and Technology Innovation Development Doubling Program of Guangxi University under Grant 2023BZRC019, in part by the Guangxi Natural Science Foundation of China under Grant 2022GXNSFAA035548, and in part by the National Key Research and Development Program of China under Grant 2022YFC3103105 and Grant 2022YFC3103100. *(Xiuling Zuo and Juncan Teng contributed equally to this work.) (Corresponding authors: Xiuling Zuo; Kefu Yu.)*

Xiuling Zuo, Juncan Teng, and Zhengxian Duan are with the Guangxi Laboratory on the Study of Coral Reefs in the South China Sea, School of Marine Sciences, Guangxi University, Nanning 530004, China (e-mail: zuoxl@gxu.edu.cn; juncanteng@st.gxu.edu.cn; 20151004114@cug.edu.cn).

Fenzhen Su is with the State Key Laboratory of Resources and Environmental Information System, Institute of Geographic Sciences and Natural Resources Research, Chinese Academy of Sciences, Beijing 100101, China (e-mail: sufz@lreis.ac.cn).

Kefu Yu is with the Guangxi Laboratory on the Study of Coral Reefs in the South China Sea, School of Marine Sciences, Guangxi University, Nanning 530004, China, and also with the Southern Marine Science and Engineering Guangdong Laboratory, Guangzhou 511458, China (e-mail: kefuyu@scsio.ac.cn).

This article has supplementary downloadable material available at https://doi.org/10.1109/JSTARS.2024.3523296, provided by the authors.

Digital Object Identifier 10.1109/JSTARS.2024.3523296

I. Introduction

SCLERACTINIAN corals are the foundation of the structure and biodiversity of coral reef ecosystems [1]. Water depth affects seawater temperature, solar radiation, and hydrodynamic energy. Therefore, the growth rate, distribution pattern, and morphology of scleractinian corals are significantly correlated with water depth [2], [3], [4], [5], [6], [7]. Currently, scleractinian corals are experiencing rapid degradation owing to both climate change and human activities [8], [9]. An accurate bathymetric map is essential in evaluating, protecting, and restoring coral reef habitats.

Conventional field bathymetry surveys are costly and challenging in remote and large-scale coral reefs, and therefore, airborne LiDAR, shipborne echosounders, and satellite images have recently been developed for bathymetry inversion in coral reefs [10]. Among them, satellite-derived bathymetry (SDB) methods are widely applied because they are highly cost-effective, broad area coverage, and are not limited by time and region [11]. SDB is typically categorized into physics-based methods and statistical methods [12], [13]. Physics-based SDB methods construct a physical optics model between water depth and spectral reflectance based on radiative transfer theory [14], [15], [16]. These models do not require any in situ data but many optical parameters, and the model algorithm is complex to construct. Statistical SDB methods use an empirical and hypothetical mathematical regression model as the correspondence between satellite spectral values and in situ bathymetry data [12], [17], which include parametric models (PMs) and nonparametric models [18]. Although these methods have been widely applied because of their advantages of convenient operation and simple calculation, their high dependence on field survey data limits their application in deriving large-scale bathymetry in coral reef habitats [17], [19], [20].

Launched in September 2018, the Ice, Cloud, and Land Elevation Satellite-2 (ICESat-2), which carries the advanced topographic laser altimeter system (ATLAS), offers new prospects for expanding the application scope of statistical SDB methods. By merging active ICESat-2 data and passive multispectral satellite images, studies suggested that the small-scale statistical SDB method can be extrapolated to other coral reefs that are close by and have similar water transparency [21], [22], [23], [24], [25], [26]. Although these active–passive studies retrieved more accurate bathymetry in shallow areas of coral reefs, the accuracy was still poor (RMSE>0.95 m) in the deeper water (>5 m) because they constructed only one SDB model for the entire coral reef area within different depth ranges [27]. In addition, these methods did not consider the effect of the substrate spectrum on bathymetry inversion. Because it is affected by high or low benthic spectral values, the water depth inverted from satellite images was underestimated or overestimated between different benthic types [28], [29], [30], [31], [32]. For example, pixels with bright sand would be predicted as shallower than coral pixels which have lower reflectance at the same depth. The significant heterogeneity in the substrates is the main reason why high-precision bathymetry inversion is more challenging in coral reef habitats than in other marine areas [33]. Owing to the diversity of reef types and benthic types in large-scale reef areas, the existing active–passive fusion SDB methods based on one model have low accuracy when directly extrapolated to derive large-scale bathymetry data.

Studies have shown that geomorphology is a key factor affecting substrate distribution and bathymetry patterns in large coral reef areas [34]. The satellite band spectrum mainly reflects the difference in benthic types in shallow geomorphic zones such as the reef flat (depth 0.5–2 m), while it mainly reflects the water depth variation information in deeper geomorphic zones such as reef slope and lagoon. However, the band reflectance values in the same water depth can vary markedly, e.g., a sand-dominated lagoon slope will have significantly higher values than those of the outer reef slope. Although the effect of the benthic spectrum on the bathymetry inversion can be reduced by adjusting the band logarithmic ratio of PMs [17], [22], [30], [35], or using nonparametric machine learning models [27], [32], one bathymetry inversion model constructed for an entire reef can only achieve high accuracy in some of the reef geomorphic zones. In the Indo-Pacific reef habitats, studies suggest that the spatial pattern of scleractinian corals, macroalgae, terrain, etc., are characterized by small differences within the same geomorphic zone but significant differences between different geomorphic zones [7], [36]. Based on ICESat-2 data and multispectral satellite images, the combination of multiple optimal bathymetry inversion models for each geomorphic zone will take into account both substrate distribution and bathymetry pattern, which may help to obtain more accurate water depth data for large coral reef areas.

Here, we used ICESat-2 data and Gaofen-1 (GF-1) medium- and WorldView-2/3 (WV-2/3) high-resolution multispectral satellite images to propose a parametric multimodel combination approach based on geomorphic segmentation (PMCGS) to obtain the water depth in the Xisha Islands (ocean area of approximately 607 km^2) in the South China Sea section of the Indo-Pacific reef region. In this methodology, we trained five parametric SDB models in each geomorphic zone by combining ICESat-2 and multispectral satellite images. Then, the optimal SDB models of each geomorphic zone were combined and extrapolated to the same geomorphic zones of 11 coral reefs to invert large-scale bathymetry. This study aimed to 1) establish the optimal bathymetry model for each geomorphic zone using active–passive remote sensing data to improve the accuracy of water depth inversion in coral reef areas and 2) verify the extrapolation feasibility of the PMCGS to derive large-scale water depths for coral reef areas where ICESat-2 data are not available. This article can provide a methodological reference for obtaining high-precision water depth data in large-scale coral reef areas, to assist with the protection and management of coral reefs.

II. Study Area and Data

A. Study Area

The 11 coral reefs in the Xisha Islands in the South China Sea were selected as the study area to demonstrate the bathymetry inversion performance of our method [see Fig. 1(a)]. These reefs include the big Yongle Atoll constituted of seven reefs, Huaguang Reef, Panshi Islet, Yuzhuo Reef, and Qilian Islet. The Xisha Islands are located in the northwestern South China Sea. This archipelago has more than 30 atolls and table reefs. The coral reefs of the Xisha Islands belong to the Indo-Pacific coral reefs and have developed complete and regular geomorphic zones [7]. Because the seawater is clear, bathymetry inverted from an optical satellite can reach approximately 30 m in these areas.

The study area was divided into following three regions.

1) Using ICESat-2 and GF-1 satellite image with 16 m resolution, a combination of optimal models was constructed in the west of Huaguang Reef [see Fig. 1(b)] and extrapolated to the 11 reefs in the Xisha Islands [see Fig. 1(a)].
2) Using ICESat-2 and WorldView-2 (WV-2) satellite image with 2 m resolution, a combination of optimal models was constructed in the east of Lingyang Reef and extrapolated to the entire Lingyang Reef [see Fig. 2(a)].
3) Using ICESat-2 and WorldView-3 (WV-3) satellite image with 2 m resolution, a combination of optimal models was constructed in the west of Qilian Islet and extrapolated to the entire Qilian Islet [see Fig. 2(c)]. Reef sections with in situ bathymetry data in GF-1 [see Fig. 1(c)–(f)] and WV-2/3 [see Fig. 2(b) and (d)] were used to evaluate our proposed bathymetry inversion approach.

B. Data

1) Field Survey Data: Water depth and geomorphic data were surveyed in eight reefs of Xisha Islands from 4 June 2013 to 29 June 2015, including Huaguang Reef, Panshi Islet, Lingyang Reef, Qilian Islet, Yinyu, Quanfu Island, Ganquan Island, and Yuzhuo Reef. Water depth was measured by a Hi-Target HD-370 depth sounder with 10 m positional accuracy and 0.3 m depth

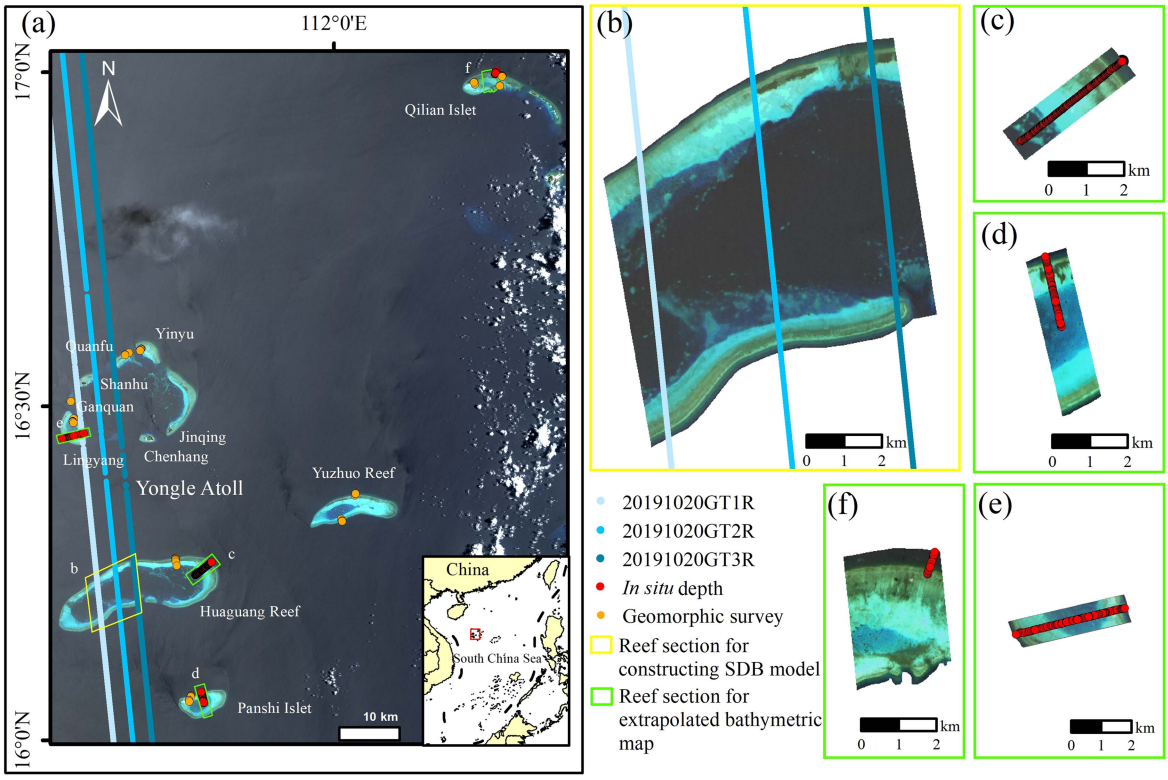

Fig. 1. (a) True-color image of the 11 coral reefs in Xisha Islands derived from GF-1 image. The inset image in the lower right corner shows the location of the study area in the South China Sea. (b) West of Huaguang Reef, where the SDB models were constructed with ICESat-2 ground tracks. Then, a combination of optimal models was extrapolated to 11 reefs in the Xisha Islands (a). Reef sections with in situ bathymetry data in (c) the east of Huaguang Reef, (d) the middle of Panshi Islet, (e) the south of Lingyang Reef, and (f) the west of Qilian Islet were presented to evaluate the accuracy of the bathymetry models. Three blue dotted lines represent ICESat-2 ground tracks: 20191020GT1R, 2R, 3R. Red dotted points represent in situ water depth data. Orange dots represent the in situ geomorphic survey data.

accuracy, which was used to validate the extrapolated accuracy of bathymetry inversion. A geomorphic survey of 20 m line transects was conducted using a video camera through SCUBA according to the interesting geomorphic sites. Prior to the field survey, a Landsat-8 image was downloaded for preliminary geomorphic presegmentation. Interested geomorphic survey sites with diverse substrates were selected based on different spectral brightness, which represented the various benthic environments within the geomorphic zones. For example, dark areas of the reef are usually regarded as corals, dense algae, or seagrass, while bright areas are sand or clouds. Fifty-four in situ geomorphic sites were surveyed [see Fig. 1(a)]. The actual geomorphic zone of each survey site was distinguished according to the environmental characteristics of substrate, water depth, and location.

2) Satellite Images: GF-1 and WV-2/3 satellite images were selected to construct the bathymetry inversion models combined with the ICEsat-2 data. The GF-1 image that covered the Xisha Islands was acquired on 30 May 2014 with a tide of 1.61 m and was obtained from the China Resource Satellite Application Center. It had four multispectral bands: blue, green, red, and near-infrared. The WV-2 image covering Lingyang Reef was acquired on 9 September 2014 with a tide of 1.20 m, and the WV-3 image covering Qilian Islet was acquired on 10 October 2014 with a tide of 0.88 m.

3) ICESat-2 Data: ICESat-2 ATLAS measures the distance to the ground at 10 kHz repetition frequency (∼70 cm sampling distance) with three pairs of 532 nm green laser beams (90 m between a dual set and 3.3 km between pairs). ATL03 is the Level-2 Global Geolocated Photon Dataset, which includes six "GTx" groups corresponding to six laser beam ground tracks. In clear seawater, photons can reach 40 m depth with a root mean square error (RMSE) of 0.43–0.89 m [22], [25], [37]. We obtained ATL03 data from the EarthData website[1] to use as control points for constructing bathymetry inversion models. Because ICESat-2 has been collecting data since 2018, three ground tracks of 20191020GT1R, 2R, 3R closest to the field survey in time were downloaded and used for constructing models with the GF-1 in the west of Huaguang Reef. The tracks of 20200419GT3R in the east of Lingyang Reef and 20191016GT2R in the west of Qilian Islet were downloaded for constructing the SDB models with WV-2/3 images, respectively. In addition, because in situ bathymetric validation datasets were available only in the reef slope of Qilian Islet, 131 ICEsat-2 bathymetric points of 20210413GT1R [see Fig. 2(c)] were extracted as water depth validation data in the reef flat and shallow lagoon.

[1][Online]. Available: https://search.earthdata.nasa.gov/search.

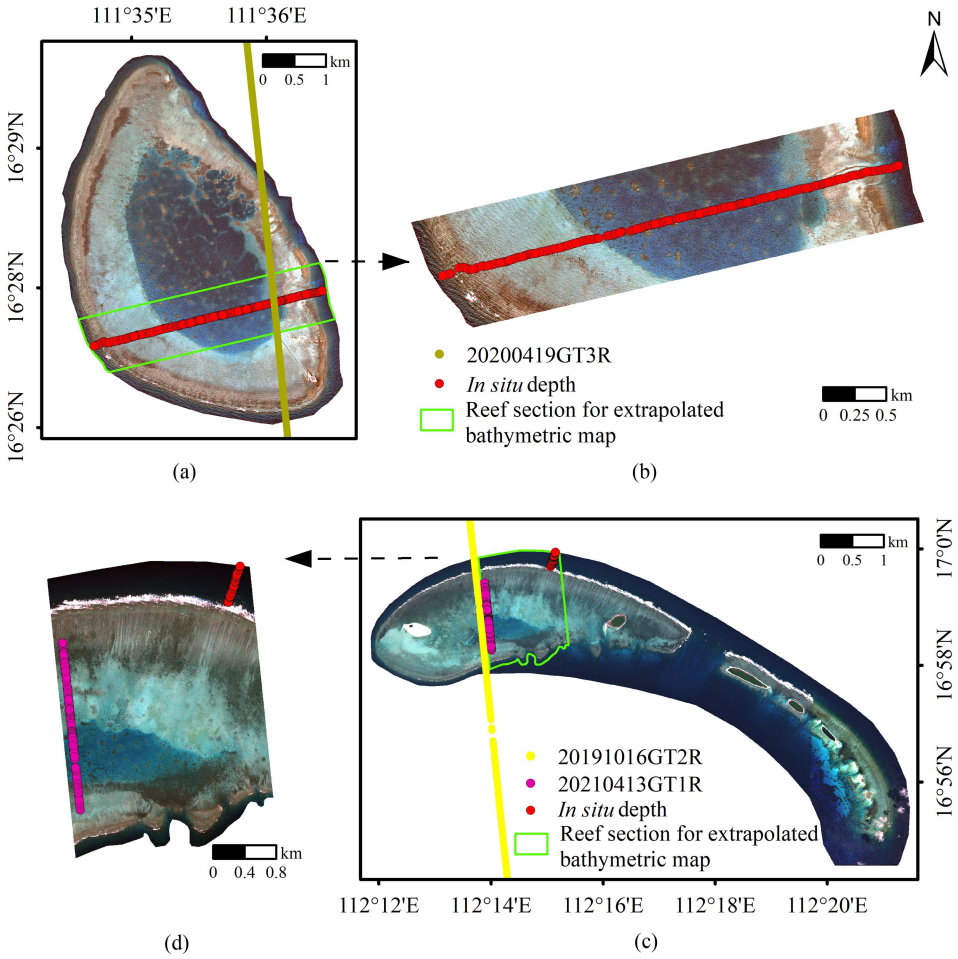

Fig. 2. (a) True-color image of Lingyang Reef derived from WV-2 image. The eastern ICESat-2 ground track (brown dotted line) was used to construct SDB models, and then a combination of optimal models was extrapolated to the Lingyang Reef (a) for bathymetry inversion. (c) True-color image of Qilian Islet derived from WV-3 image. The western ICESat-2 ground track (yellow dotted line) was used to construct SDB models, and then a combination of optimal models was extrapolated to the Qilian Islet (c) for bathymetric inversion. Reef sections with in situ bathymetry data in (b) the south of Lingyang Reef and (d) the west of Qilian Islet were presented to evaluate the accuracy of the bathymetry models. The in situ depth (red dotted line) and the ICESat-2 ground track of 20210413GT1R (pink dotted line) in (d) are validation data of Qilian Islet.

III. Methods

The overall technical framework diagram is shown in Fig. 3. First, the GF-1 and WV-2/3 satellite images and ICESat-2 ATL03 data were preprocessed and used to construct SDB models. Second, according to our proposed PMCGS approach, five PMs were trained for five geomorphic zones, and the optimal models of each geomorphic zone were combined and extrapolated to large regions for bathymetry inversion. To compare with the PMCGS, a one-model approach was used, in which one PM and three nonparametric machine learning models were constructed throughout the entire area without geomorphic segmentation and extrapolated to the same regions as the PMCGS approach. Finally, the extrapolated bathymetric results were validated with in situ water depth.

A. Field Data Processing

Tide correction was conducted for in situ water depth data to the imaging time of satellite images according to the tide table of the Xisha Islands. A pixel could contain multiple depth points because the spatial resolution of in situ water depth sample points was higher than satellite images. Thus, all in situ water depth points within the same pixel were averaged using ArcGIS 10.7 prior to bathymetry inversion. Finally, each mean depth corresponded to a pixel, and the down-sampled in situ water depth data were used to validate the proposed bathymetry inversion method.

B. Satellite Image Processing

Satellite images were processed for radiometric calibration and atmospheric correction using the FLAASH model in ENVI 5.3. Based on the panchromatic band of the Landsat-8 satellite image, the GF-1 image was geometrically corrected. Then, the pixels covered by land areas were removed [38]. Because regional reflectance differences in the deep-sea pixels existed in the GF-1 image, the band reflectance values of the GF-1 image in the Xisha Islands were corrected based on the reflectance value

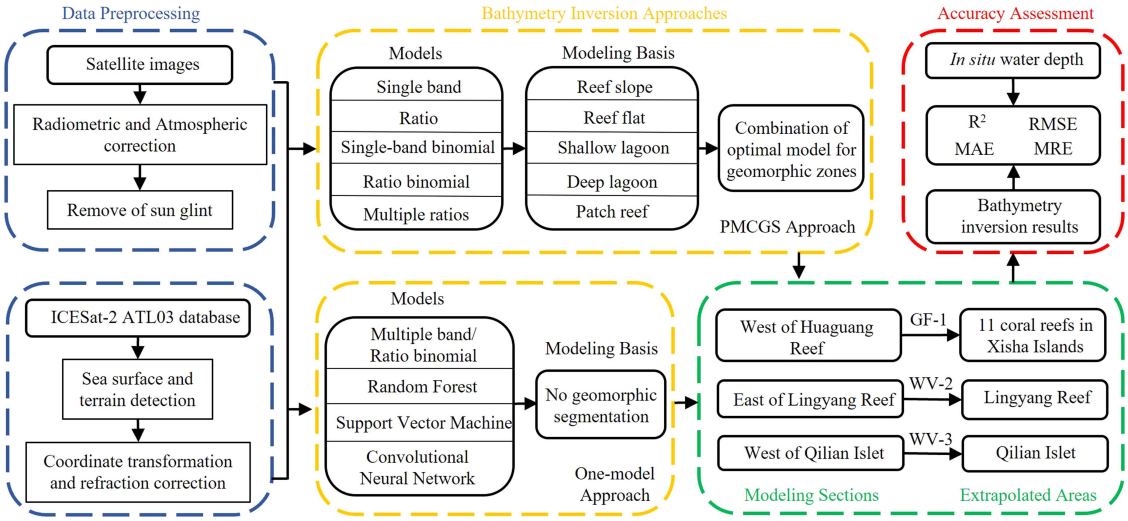

Fig. 3. Technical framework diagram.

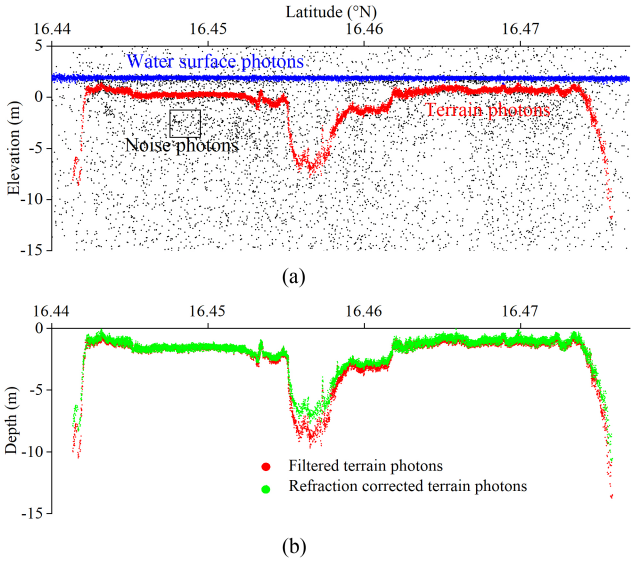

Fig. 4. Example of ICESat-2 data processing of the 20200419GT3R ground track in the south of Lingyang Reef. (a) Raw point cloud, which includes noise (black), seawater surface (blue), and terrain photons (red). (b) Transformation of datum from ellipsoidal height (a) to water depth relative to the mean sea surface. Terrain photons in (b) (red) were filtered out from (a), and then they were further corrected for refraction (green).

of deep-sea pixels in the Qilian Islet. In addition, the effects of sun glint in the WV-2 were removed using the technique developed by Hedley et al. [39].

C. ICESat-2 ATL03 Data Processing

The ground track of 20200419GT3R in Lingyang Reef was used as an example to demonstrate the processing steps (see Fig. 4). First, according to the principle that the point cloud density of noise is low and the signal is high, the terrain photons and sea surface photons were filtered manually [40] [see Fig. 4(a)]. Second, the ICESat-2 ATL03 data were transformed from WGS84 ellipsoid height to water depth relative to mean sea level. Because laser beams refract as they pass through the air–sea interface, terrain photons must be further corrected to obtain accurate water depth [see Fig. 4(b)]. The algorithm of refraction correction referred to Xie et al. [41] and was calculated according to Snell's Law. Finally, the tide correction was also conducted on these ICEsat-2 data, and down-sample processes were the same as in Section III-A. In this study, 224 ICESat-2 bathymetric points in the west of Huaguang Reef, 1346 points in the east of Lingyang Reef, and 834 points in the west of Qilian Islet were extracted and used for training their SDB models, respectively.

D. Geomorphic Mapping

The geomorphic map of coral reefs in the Xisha Islands was adopted, which was visually interpreted by Zuo et al. [7] using the same GF-1 image and mapped eight geomorphic zones for emergent reefs. According to the geomorphic segmentation scheme (Supplementary material, Table S1), we merged the geomorphic categories into five classes in ArcGIS 10.7, which were reef slope, reef flat, shallow lagoon, deep lagoon, and patch reef (see Fig. 5). Finally, the accuracy of the geomorphic map was verified by the in situ geomorphic data (see Fig. 1), and the overall accuracy and Kappa were 91% and 87% in the confusion matrix (Supplementary material, Table S2), respectively.

E. Parametric Multimodel Combination Bathymetry Inversion Approach Based on Geomorphic Segmentation

ICESat-2 depth points and satellite multispectral pixels were spatially paired up to construct bathymetry inversion models based on geomorphic segmentation, and the optimal model in each geomorphic zone was combined for bathymetry inversion. In this study, five parametric SDB models were tested in each geomorphic zone: single band model (1), ratio model (2), single-band binomial model (3), ratio binomial model (4), and multiple ratios model (5). These parametric SDB models were

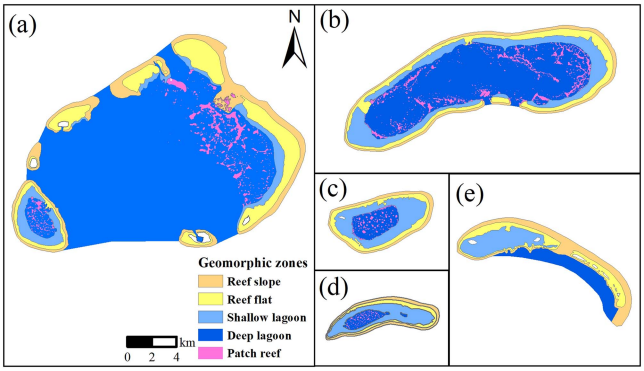

Fig. 5. Geomorphic classification map of 11 coral reefs in the Xisha Islands. (a) Seven reefs of Yongle Atoll. (b) Huaguang Reef. (c) Panshi Islet. (d) Yuzhuo Reef. (e) Qilian Islet.

constructed in three regions, which were the west section of Huaguang Reef with GF-1 [see Fig. 1(b)], the east section of Lingyang Reef with WV-2 [see Fig. 2(a)], and the west section of Qilian Islet with WV-3 [see Fig. 2(c)]. The equations and rationality for adopting each parametric SDB model are listed below.

Single band model: When the substrate and water quality are homogeneous, spectral reflectance is only related to water depth and they have a log-linear relationship [17]

$$D = a \times \ln R(\lambda_i) + b. \tag{1}$$

Ratio model: The spectral reflectance varies significantly with substrate types, but the ratio of spectral reflectance remains constant and is only related to the water depth [35]

$$D = a \times \frac{\ln R(\lambda_i)}{\ln R(\lambda_j)} + b. \tag{2}$$

Single-band binomial model and ratio binomial model: The reflectance of the single-band or band ratio to water depth is a nonlinear binomial relationship [42]

$$D = a \times [\ln R(\lambda_i)]^2 + b \times \ln R(\lambda_i) + c \tag{3}$$

$$D = a \times \left[\frac{\ln R(\lambda_i)}{\ln R(\lambda_j)}\right]^2 + b \times \frac{\ln R(\lambda_i)}{\ln R(\lambda_j)} + c. \tag{4}$$

Multiple ratios model: One reflectance ratio has the limited ability to reduce the influence of substrate types, but multiple reflectance ratios can further reduce the influence [30]

$$D = \sum_{i=1}^{n}\sum_{j=1}^{n}\left[a_{ij} \times \frac{\ln R(\lambda_i)}{\ln R(\lambda_j)}\right] + b_{ij}. \tag{5}$$

In the above equations, R_i and R_j are the processed reflectance logarithm of i and j bands, and a, b, c, a_{ij}, b_{ij} are the statistical coefficients. All band combination types were tested in modeling.

F. One-Model Approaches Without Geomorphic Segmentation for Comparison

For comparison with our PMCGS approach, the one-model approach was conducted without geomorphic segmentation, in which one PM and three nonparametric machine learning models were tested. We used the same training and validation data with the PMCGS. First, referring to Zhang et al. [23] and Cao et al. [21], respectively, a multiple band model was trained in the west of Huaguang Reef [see Fig. 1(b)] based on GF-1 and in the east of Lingyang Reef [see Fig. 2(a)] based on WV-2. Referring to Li [19], a ratio binomial model was trained in the west of Qilian Islet [see Fig. 2(c)] based on WV-3. Second, three nonparametric machine learning models using random forest (RF), support vector machine (SVM), and convolutional neural network (CNN) were constructed using *randomForest*, *e1071,* and *keras3* package in R 4.4.1, respectively. All machine learning models were adjusted and tested, and the optimal results were retained. The model parameters are shown in Supplementary material Table S3.

G. Extrapolation and Accuracy Assessment of Bathymetry Inversion Approaches

The PMCGS model and one-model approaches were all extrapolated to other coral reefs outside the training area. Models constructed in the west of Huaguang Reef [see Fig. 1(b)] were extrapolated to the 11 coral reefs in Xisha Islands [see Fig. 1(a)] based on the GF-1. Models constructed in the east of Lingyang Reef [see Fig. 2(a)] and west of Qilian Islet [see Fig. 2(c)] were extrapolated to the entire Lingyang Reef and Qilian Islet based on the WV-2/3. For GF-1 image, four reef sections with in situ bathymetry data, including the east of Huaguang Reef [see Fig. 1(c)], the middle of Panshi Islet [see Fig. 1(d)], the south of Lingyang Reef [see Fig. 1(e)], and the west of Qilian Islet [see Fig. 1(f)] were presented to show the bathymetry inversion results and the accuracy. For WV-2/3 high-resolution images, accuracy evaluation was conducted on the south section of Lingyang Reef [see Fig. 2(b)] with in situ bathymetry data and on the west section of Qilian Islet [see Fig. 2(d)] with approximately 20% in situ and 80% ICESat-2 bathymetry data.

The bathymetry inversion accuracy of SDB models was evaluated from three aspects (overall, depth segments, and geomorphic zones) by the fitting regression coefficient R^2, RMSE, mean absolute error (MAE), and mean relative error (MRE). Finally, the overlapping bathymetric paths of in situ and SDB in Lingyang Reef and Qilian Islet were extracted to compare the model performance between GF-1 and WV-2/3

$$R^2 = 1 - \frac{\sum_{i=1}^{N}(Z_d - Z_v)^2}{\sum_{i=1}^{N}(Z_v - Z_a)^2} \tag{6}$$

$$\text{RMSE} = \sqrt{\frac{1}{N}\sum_{i=1}^{N}(Z_d - Z_v)^2} \tag{7}$$

$$\text{MAE} = \frac{1}{N}\sum_{i=1}^{N}|Z_d - Z_v| \tag{8}$$

$$\text{MRE} = \frac{1}{N}\sum_{i=1}^{N}\frac{|Z_d - Z_v|}{Z_v} \times 100\% \tag{9}$$

where Z_d is water depth data inverted from satellite image. Z_v is in situ or ICESat-2 validated water depth data. Z_a is the average

TABLE I
FITTED REGRESSION COEFFICIENTS R^2 OF FIVE PARAMETRIC SDB MODELS IN EACH GEOMORPHIC ZONE IN SECTIONS OF WEST OF HUGUANG REEF (GF-1), EAST OF LINGYANG REEF (WV-2), AND WEST OF QILIAN ISLET(WV-3)

Reef section of the bathymetry model constructed (sensor type)	Geomorphic zone	Single band model	Ratio model	Single-band binomial model	Ratio binomial model	Multiple ratios model
West of Huaguang Reef (GF-1)	Reef slope	0.87	0.73	0.95	**0.96**	0.89
	Reef flat	0.52	0.58	0.72	0.59	**0.89**
	Shallow lagoon	0.72	0.82	0.84	0.85	**0.91**
	Deep lagoon	0.91	0.97	0.97	**0.98**	0.97
	Patch reef	0.8	0.8	0.72	0.72	**0.84**
East of Lingyang Reef (WV-2)/West of Qilian Islet (WV-3)	Reef slope	0.46/0.76	0.80/0.91	0.51/0.79	**0.86/0.93**	0.84/0.92
	Reef flat	0.38/0.31	0.75/0.60	0.46/0.34	0.75/0.60	**0.83/0.65**
	Shallow lagoon	0.26/0.71	0.76/0.96	0.28/0.88	0.76/0.96	**0.82/0.97**
	Deep lagoon	0.89/-	0.47/-	**0.91/-**	0.47/-	0.53/-
	Patch reef	0.81/-	0.70/-	0.83/-	0.73/-	**0.93/-**

(Bold indicates the optimal model with the highest R^2. Note that the section west of Qilian Islet does not have deep lagoon and patch reef zones.)

of in situ or ICESat-2 validated water depth data. N is the number of samples.

IV. RESULTS

A. Optimal Models in Geomorphic Zones

The R^2 of five bathymetry models in each geomorphic zone is shown in Table I. Taking the model with the highest R^2 as optimal, we found that the multiple ratios model was optimal for the reef flat, shallow lagoon, and patch reef zones for GF-1 and WV-2/3 images. The single-band binomial and the ratio binomial models were optimal for the reef slope and deep lagoon zones for GF-1 and WV-2/3 images. These optimal models in each geomorphic zone (Supplementary Material, Table S4) were combined to constitute our PMCGS approach.

B. GF-1 Bathymetry Inversion

Using PMCGS approach, the bathymetric maps derived from the GF-1 image were presented in the east section of Huaguang Reef [see Fig. 6(a)], the middle section of Panshi Islet [see Fig. 6(b)], the south section of Lingyang Reef [see Fig. 6(c)], and the west section of Qilian Islet [see Fig. 6(d)]. Evaluation with in situ data suggested that the PMCGS inverted bathymetry in GF-1 image had an RMSE of 0.91 m, MAE of 0.62 m, and MRE of 13.06% [see Fig. 7(a)], which had significantly higher accuracy than the one-model approaches without geomorphic segmentation [see Fig. 7(d), (g), (j), (m)]. In the one-model approaches, the PM had an RMSE of 1.88 m [see Fig. 7(d)], and the nonparametric machine learning models had RMSEs between 2.21 and 2.46 m [see Fig. 7(g), (j), (m)].

Bathymetric profiles using the PMCGS approach reflected the characteristics of each geomorphic zone [see Fig. 6(e)–(h)]. Reef slope terrain was extremely steep and the water depth dropped rapidly from 1 to 20 m over a short distance. The steepness was ranked as south of Lingyang Reef > middle of Panshi Islet > west of Qilian Islet > east of Huaguang Reef. The bathymetry of reef flat and shallow lagoon was 2–3 m. The deep lagoon of the east of Huaguang Reef was the deepest at approximately 20 m. Patch reefs rose vertically and were unevenly distributed within the lagoon. The patch reefs of the east of Huaguang Reef resembled a peak with a sharp top and two steep sides, while those of the south of Lingyang Reef and the middle of Panshi Islet resembled a mound with a rounded top and two gently sloping sides.

C. WV-2/3 Bathymetry Inversion

Using the PMCGS approach, extrapolated bathymetric maps and profiles derived from WV-2/3 were presented in the south of Lingyang Reef and the west of Qilian Islet (see Fig. 8). Evaluation using the in situ data suggested that the PMCGS inverted bathymetry had an RMSE of 0.70 m, MAE of 0.50 m, and MRE of 11.99% in Lingyang Reef [see Fig. 7(b)]. Evaluation using the in situ and the ICESat-2 data, the PMCGS inverted bathymetry in Qilian Islet had an RMSE of 0.88 m, MAE of 0.52 m, and MRE of 16.38% [see Fig. 7(c)]. Using the one-model approaches without geomorphic segmentation, the water depth inverted by PMs had an RMSE of 1.70 m in the Lingyang Reef [see Fig. 7(e)] and 1.12 m in the Qilian Islet [see Fig. 7(f)], respectively. The water depth inverted by machine learning models had RMSEs from 1.13 to 1.88 m [see Fig. 7(h), (i), (k), (l), (n), (o)]. Thus, the PM (RMSE = 1.12 m) outperformed nonparametric machine learning models (RMSE = 1.36–1.51 m) in Qilian Islet, although it performed worse (RMSE = 1.70 m) than the machine learning models (RMSE = 1.13–1.46 m) in Lingyang Reef, except for the CNN model.

In summary, the PMCGS outperformed the one-model approaches without geomorphic segmentation. Besides, the bathymetry inverted from WV-2/3 was more accurate than that from GF-1 image (see Fig. 7). Finer terrain changes from the

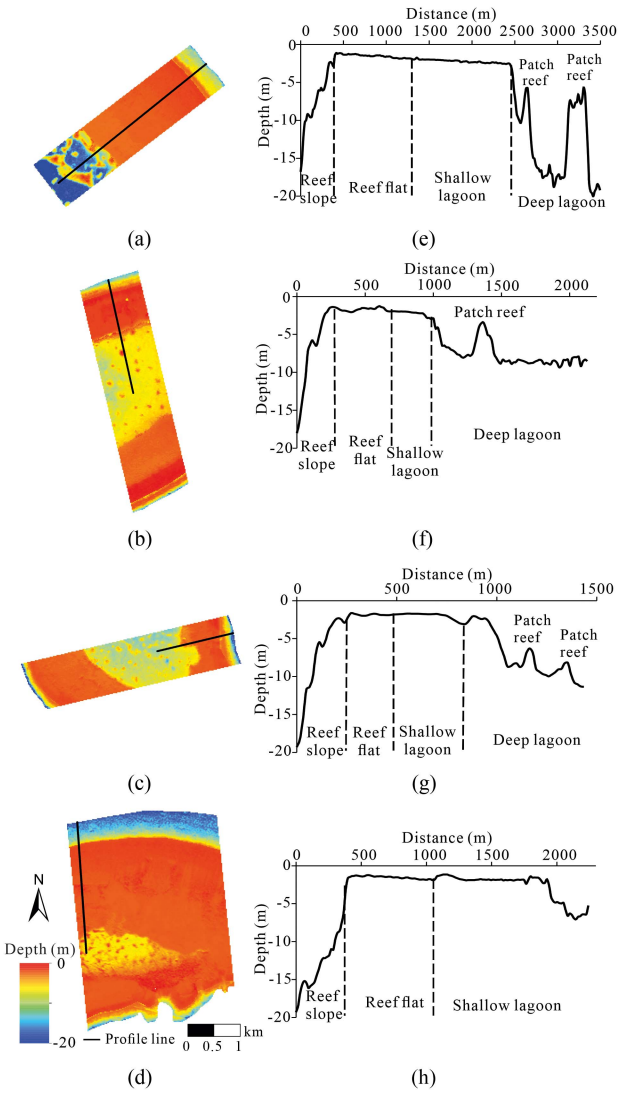

Fig. 6. Bathymetric maps and profiles derived from GF-1 using the PMCGS approach. Study areas were (a) the east of Huaguang Reef, (b) the middle of Panshi Islet, (c) the south of Lingyang Reef, and (d) the west of Qilian Islet. (e)–(h) Bathymetric profiles corresponding to (a)–(d), respectively, from the reef slope to the lagoon.

reef slope to the lagoon can be identified from WV-2/3 images (see Fig. 8) than from GF-1 image (see Fig. 6).

D. Accuracy of the PMCGS Approach in Different Depth Segments and Geomorphic Zones.

The comparison of the water depth data inverted from medium- and high-resolution images at overlapping paths suggested that the bathymetry derived from WV-2/3 images better matched in situ data than that from GF-1 image, both in the south of Lingyang Reef [see Fig. 9(a)] and in the west of Qilian Islet [see Fig. 9(b)]. The performance differences between WV-2/3 and GF-1 were particularly noticeable in the reef slope and the deep lagoon. The accuracy still varied in different reefs, depth segments, and geomorphic zones.

The accuracy of the bathymetric data inverted using the PMCGS approach in each depth segment is shown in Fig. 10 and Supplementary Material, Table S5. Results suggested that the PMCGS approach performed best at 0–5 m depth, with an RMSE of 0.27–0.56 m and MAE of 0.21–0.38 m [see Fig. 10(a), (b)]. The accuracy was lowest at 10–15 m depth segment, with an RMSE of 0.96–2.44 m and MAE of 0.84–2.04 m [see Fig. 10(a), (b)]. The PMCGS approach in the WV-2/3 images performed better than in the GF-1 image at depths of 10–15 m (see Fig. 10). The MRE varied from 6.73% to 18.38% in all depth segments [see Fig. 10(c)].

The bathymetric errors in geomorphic zones showed that the PMCGS approach performed best in shallow-water geomorphic zones in both GF-1 and WV-2/3 images, such as the reef flat and shallow lagoon, with an RMSE of 0.17–0.46 m [see Fig. 11(a), Supplementary Material, Table S6). The accuracy was lowest in the reef slope, with an RMSE of 1.20–1.83 m, MAE of 1.03–1.47 m, and MRE of 13.11%–22.33% [see Fig. 11, Supplementary Material, Table S6). The bathymetric data inverted from the WV-2 image in the Lingyang Reef had the highest accuracy among all satellite images [see Fig. 11(a) and (b)].

V. Discussion

A. Optimal Bathymetry Inversion Model in Each Geomorphic Zone

The highest R^2 was used to determine the optimal model. In this process, the errors of each model were also evaluated using RMSE value to ensure the criteria of the highest R^2 was justifiable in this area. Because a poor optimal model may also have large errors but high R^2 in other study areas, we should also consider the errors for future work with this approach. Modeling results of the PMCGS indicated that the multiple ratios model was optimal for the reef flat, shallow lagoon, and patch reef (see Table I). These geomorphic zones are characterized by shallow water, flat terrain, and uniform water column optical properties in the vertical direction. However, their substrate types are highly heterogeneous and the spectra are mixed with various information, which affects the bathymetry inversion accuracy [43]. Studies found that the multiple ratios model was more effective in reducing the effects of substrate types than the single ratio model [30], [35], which is consistent with our models.

The binomial models, including the ratio binomial and single-band binomial models, were optimal for the reef slope and deep lagoon (see Table I). These geomorphic zones are characterized by deep water and rapidly changing terrain, thus the spectra predominantly carry water depth information. However, studies have shown that the assumption of vertical uniformity of the water column is no longer valid in deep water, and the signal-to-noise ratio decreases as the depth increases. Thus, the SDB accuracy decreases as water depth increases [42], [44], [45]. Another study found that increasing the polynomial degree of the SDB model better fit the relationship between depth and reflectance in deep water, which could improve SDB accuracy in deep water [46]. The study also found that binomial models were suitable for reef slopes and deep lagoons (see Table I). Therefore, the PMCGS approach has simultaneously considered the benthic and terrain variation features in different geomorphic zones, which effectively reduced SDB error.

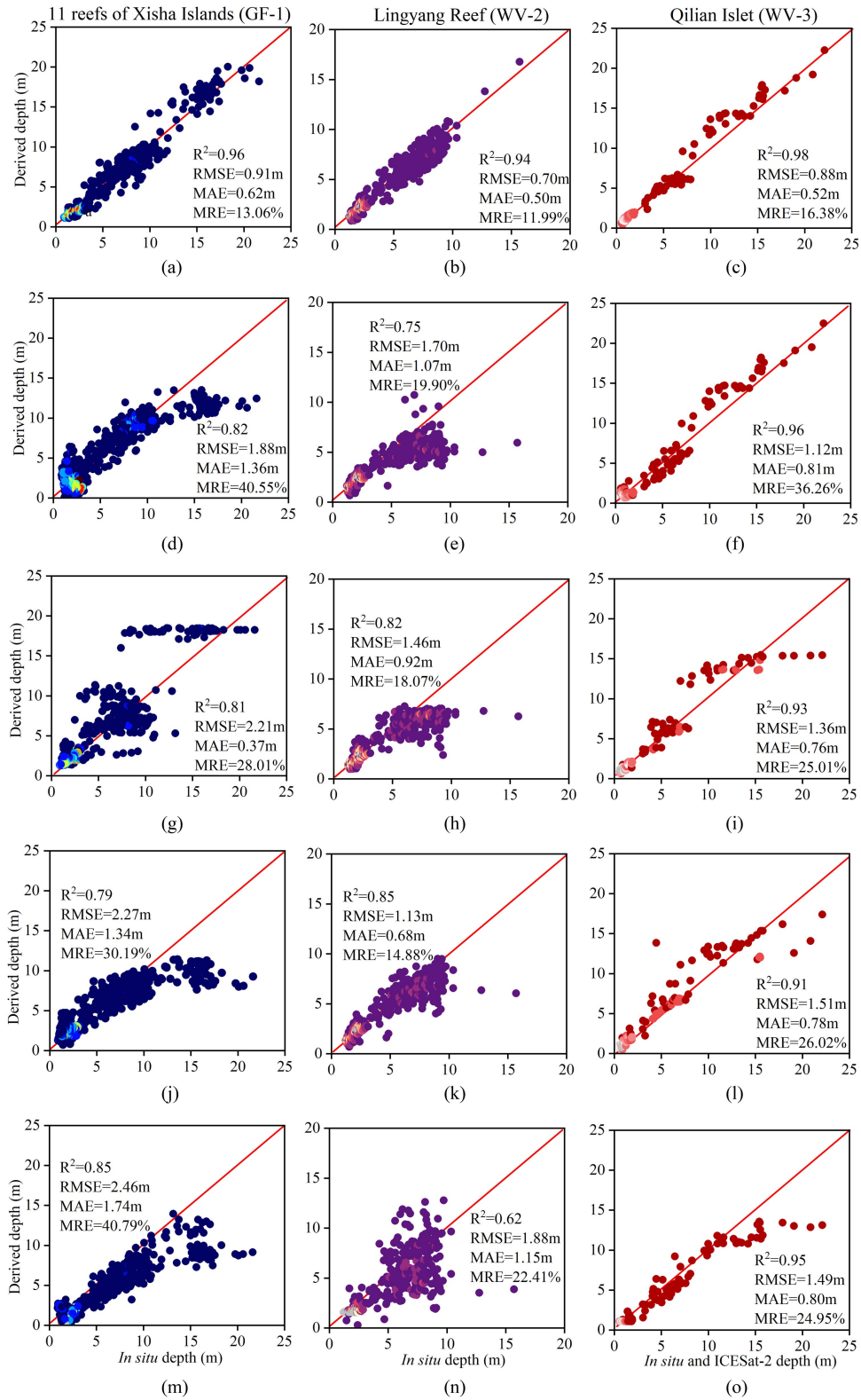

Fig. 7. Error scatter plots of derived depth versus in situ depth in the extrapolated study areas of 11 reefs of Xisha Islands (GF-1), Lingyang Reef (WV-2), and Qilian Islet (WV-3). (a)–(c) Results used the parametric multimodels combination approach based on geomorphic segmentation (PMCGS). (d)–(o) Results used the one-model approaches, where (d)–(f) used the PMs, (g)–(i) used the RF model, (j)–(l) used the SVM model, (m)–(o) used the CNN model. The red line is the 1:1 line. The color of the scatter dots represents the density, and the colors from dark to light represent the density from low to high. (a) PMCGS. (b) PMCGS. (c) PMCGS. (d) PM. (e) PM. (f) PM. (g) RF. (h) RF. (i) RF. (j) SVM. (k) SVM. (l) SVM. (m) CNN. (n) CNN. (o) CNN.

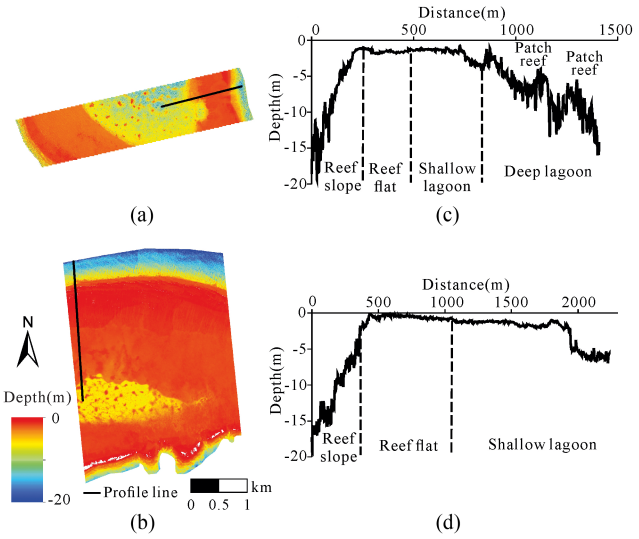

Fig. 8. Bathymetric maps and profiles derived from WV-2/3 using the PMCGS approach. Study areas were (a) the south of Lingyang Reef and (b) the west of Qilian Islet. (c) and (d) Bathymetric profiles from reef slope to lagoon corresponding to (a) and (b), respectively.

B. Comparison of the Bathymetry Inversion Approaches

In previous studies, a geographically adaptive inversion method [20] was proposed to improve the bathymetry inversion accuracy, but its extrapolating performance has not been analyzed. The PMCGS method was constructed based on the geomorphic characteristics due to complex seafloor environment of coral reefs and can extrapolate efficiently to other coral reefs, which was more accurate than the one-model methods (PM, RF, SVM, CNN) without geomorphic segmentation (see Fig. 7). To compare the PMCGS method with previous SDB methods, we referred to studies in the Xisha Islands, which used the same sensor or sensors with similar spatial resolution. Results suggested that the inverted bathymetry from GF-1 (RMSE = 0.91 m), adopting PMCGS, was more accurate than the multitemporal method (RMSE = 1.08 m) [25], and had higher accuracy than other one-model methods without geomorphic segmentation (RMSE = 0.94–1.58 m) [23], [24], [47], [48]. The inverted bathymetry from WV-2/3 (RMSE = 0.70–0.88 m) using the PMCGS approach was more accurate than the one-model approach that merged active–passive remote sensing data (RMSE = 0.931 m) [21]. The proposed PMCGS model significantly improved the bathymetric accuracy compared with the entirely one-model approaches and previous studies.

Using the one-model SDB approaches without geomorphic segmentation, previous studies found that nonparametric machine learning models generally outperformed parametric models [27], [49]. However, the parametric model outperformed the three machine learning models in the 11 reefs of Xisha Islands in GF-1 and Qilian Islet in WV-3, although it performed worse than the RF and SVM in the Lingyang Reef in WV-2 in this study (see Fig. 7). The model performance differences may be because machine learning models rely more on training sample size than parametric models. A large number of 1346 training samples were used in Lingyang Reef, while a small set of training sample points of 224 and 834 were used in 11 coral reefs in the Xisha Islands and Qilian Islet, respectively. The relationship between training data volume and model performance was further analyzed across four one-model approaches (see Fig. 12). Results showed that the errors of three machine learning models decreased as the training data volume increased, especially for the CNN model. However, no obvious relationship was found between the training data volume and the PM model performance. This is consistent with the findings of previous studies that the performances of machine learning models are affected by training sample size, while those of the parametric models are affected by sample quality [49], [18]. Owing to the limited training samples in each geomorphic zone, this relationship analysis could not be carried out for the PMCGS model. Additionally, the sensor type and study area may also cause a difference in model performances [23].

Although the nonparametric machine learning models performed poorly in this study [see Fig.7(g)–(o)], other studies found that the machine learning models could more effectively improve the SDB accuracy than parametric models in turbid and terrain-complex areas with sufficient training data volume [12], [50]. However, machine learning models require a large number of training samples, and their extrapolation to invert large-scale bathymetry is challenging in coral reef areas because of the heterogeneous substrate and terrain [27]. In contrast, the PMCGS approach proposed in this study was extrapolated effectively to other coral reefs and obtained large-scale bathymetry [see Fig. 7(a)–(c)]. Therefore, the geomorphic segmentation and machine learning models can be further combined in future research to discover whether this method can further improve the SDB model performance if more training samples are acquired. In addition, geomorphic mapping is a necessary step for the PMCGS construction. Coral reef geomorphology is influenced by geological structure, biology, hydrodynamics, and sedimentary processes. The boundaries of each zone are clear and can be accurately mapped from moderate- to high-resolution satellite images. There are many references for the geomorphic mapping of coral reefs [5], [34], [51], [52], [53]. Because Indo-Pacific coral reefs have developed complete and regular geomorphic zones, the geomorphological partitioning procedure is feasible and can be achieved universally.

C. Bathymetry Inversion Accuracy in Depth and Geomorphic Segments

The bathymetric accuracy of the proposed PMCGS was significantly higher than previous studies in the 0–5 m, 5–10 m, and 15–25 m depth segments [54], [55], while it was relatively lower at 10–15 m (see Fig. 10). The bathymetric points in the 10–15 m depth segment were further geographically analyzed. In GF-1, we found that these bathymetric points were predominantly located in the reef slope and the deep lagoon, but only the points in the reef slope deviated significantly from the in situ water depth points (Supplementary Material, Fig. S1). In WV-2/3, these bathymetric points were all located on the reef slope. In addition, the bathymetric accuracy in each geomorphic zone indicated that the reef slope was the primary error source (see

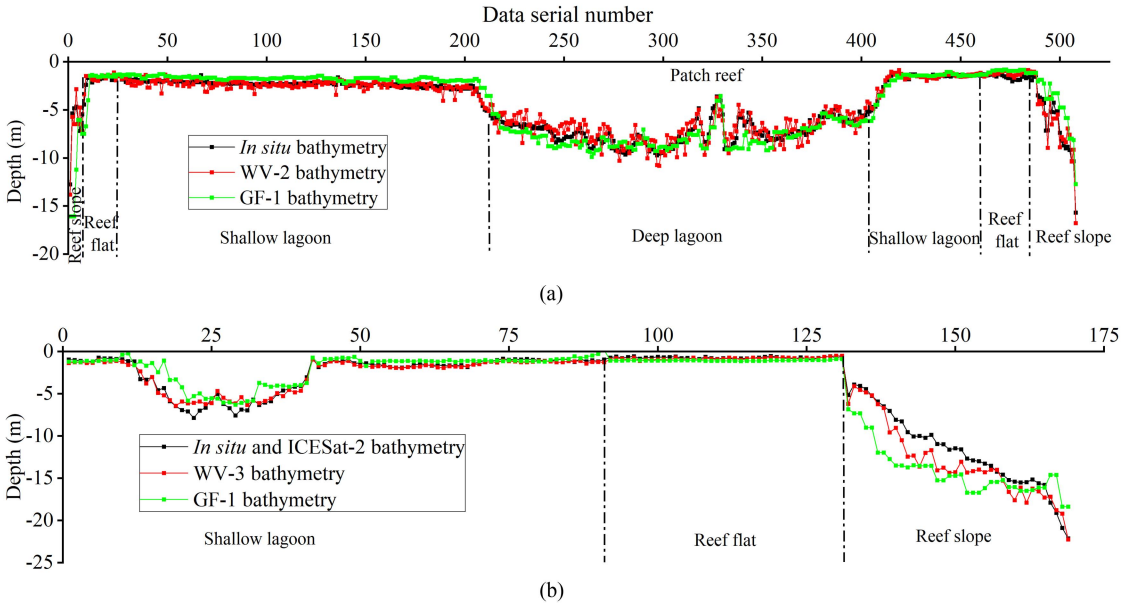

Fig. 9. Comparison of the in situ bathymetry data (black dotted line) versus satellite inverted bathymetry data (red and green dotted lines) at overlapping paths using the PMCGS approach. The paths were in (a) the south of Lingyang Reef and (b) the west of Qilian Islet. The x-axis is the serial number of bathymetric points arranged in the coral reef section, and their locations refer to Fig. 2(b) and (d).

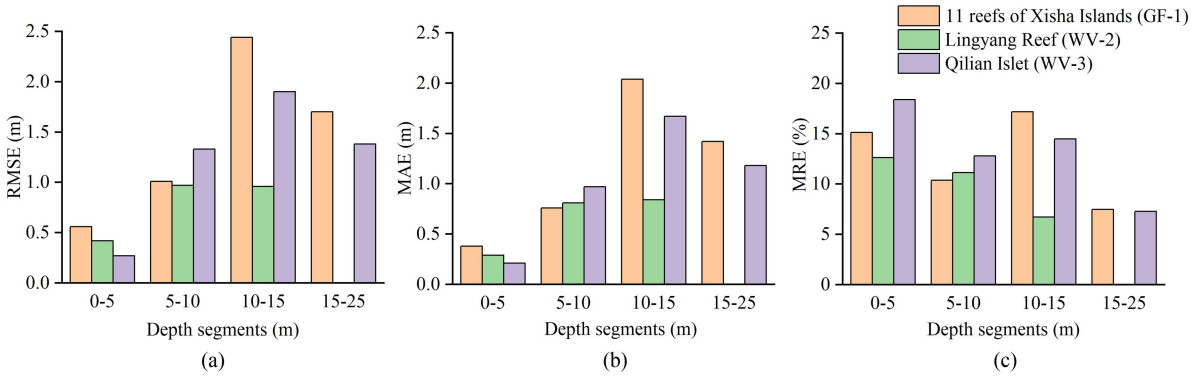

Fig. 10. Bathymetry inversion errors of different depth segments using the PMCGS approach in extrapolated areas, including the 11 reefs of Xisha Islands (GF-1), Lingyang Reef (WV-2), and Qilian Islet (WV-3). Error indexes include (a) RMSE, (b) MAE, and (c) MRE.

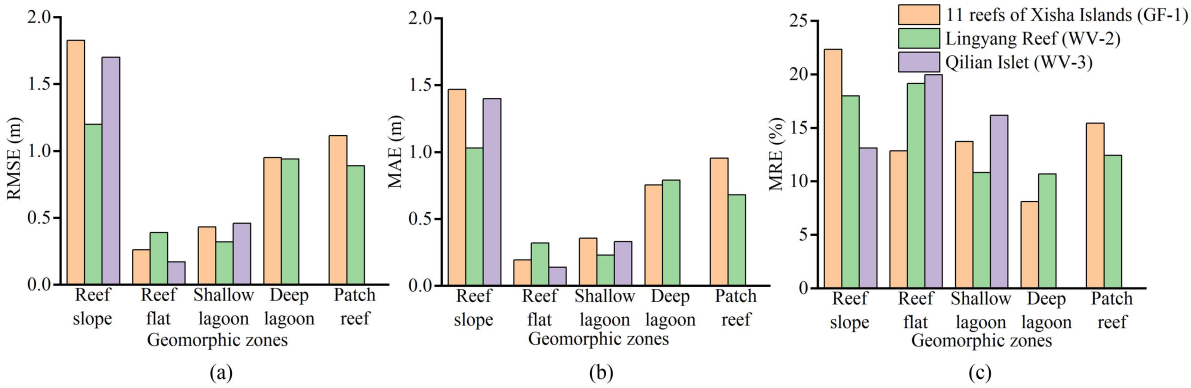

Fig. 11. Bathymetry inversion errors of different geomorphic zones using the PMCGS approach in extrapolated areas, including the 11 reefs of Xisha Islands (GF-1), Huaguang Reef (WV-2), and Qilian Islet (WV-3). Error indexes include (a) RMSE, (b) MAE, and (c) MRE.

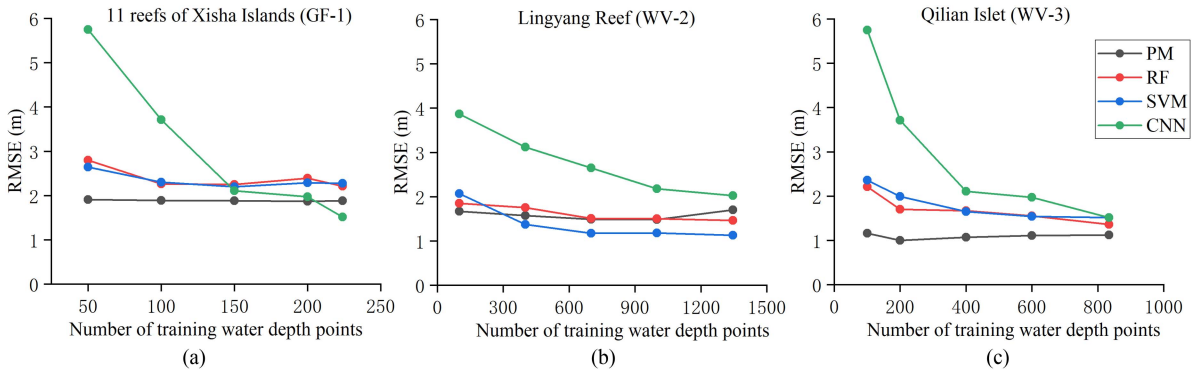

Fig. 12. Relationship between training sample size and model performance across four one-model approaches without geomorphic segmentation. Study areas were (a) 11 reefs of Xisha Island with GF-1, (b) Lingyang Reef with WV-2, and (c) Qilian Islet with WV-3. Four colors of lines represent the PM, RF model, SVM model, and CNN model, respectively.

Fig. 11). Because the reef slope is characterized by steep seafloor terrain, the geolocation-induced inverted bathymetry accuracy tends to decrease when the slope is steeper [56]. Besides, the reef slope is the deepest zone among all geomorphic zones, and the SDB accuracy generally decreases with increasing water depth because spectral reflectance was attenuated rapidly [57], [58]. Therefore, the reef slope, characterized by steep terrain and deep water, is the main zone affecting the bathymetric accuracy in the 10–15 m depth segment.

The performances of the one-model approaches without geomorphic segmentation across geomorphic zones were further compared using the RMSE value. Results showed that these four approaches had low bathymetric accuracy in most geomorphic zones (Supplementary Material, Fig. S2), except for the reef flat and shallow lagoon of Lingyang Reef and Qilian Islet, which had more training samples than those of 11 reefs of Xisha Islands. The performances of the parametric model and nonparametric machine learning models had no significant differences in shallow geomorphic zones, such as reef flat, shallow lagoon, and patch reef. However, their performances showed obvious differences in the reef slope and deep lagoon zones (Supplementary Material, Fig. S2). Overall, none of the four models analyzed performed best in all geomorphic zones, and training respective SDB models for geomorphic zones is necessary.

D. Accuracy Comparison Between GF-1 and WV-2/3

The Xisha Islands are far from human activities, and the acquisition time between GF-1 and WV-2/3 was only four months, suggesting that the terrain and water environment were nearly the same in both satellite images. In addition, no significant visual differences were observed between GF-1 and WV-2/3 true-color images. Thus, the performance differences between the WV-2/3 and GF-1 images were mostly due to the spatial resolution of the two sensors. The comparison of in situ and satellite inverted bathymetric data in overlapping paths suggested that no obvious differences were found between GF-1 and WV-2/3 in shallow water (see Fig. 9). However, the high-resolution WV-2/3 images performed better than the medium-resolution GF-1 image in bathymetry inversion in deep water, especially in the reef slope (see Fig. 9). Reef slopes have high coral diversity and steep terrain [7], and their water depth changes significantly over short distances. Thus, the pixel scale is inversely proportional to the inversion accuracy due to geolocation, which is consistent with previous studies [22], [56]. Nonetheless, the medium-resolution image is a balanced choice to simultaneously derive accurate and large-scale bathymetric maps.

E. Limitations

The SDB accuracy can be affected by the tide, sun glint, and time interval of dataset. The reef flat water depth in the west of Qilian Islet was shallower than 1 m owing to low tide, thus the WV-3 image spectra carried mostly substrate information instead of water depth, which resulted in an $R^2 = 0.65$ for the optimal bathymetry inversion model (see Table I). In addition, the WV-2 image of Lingyang Reef was affected severely by sun glint, and some abnormal pixels still existed even after the removal of sun glint, which may also affect the bathymetric accuracy. Thus, to derive accurate bathymetric maps, we suggest that high-quality satellite images taken at high tide should be used as much as possible.

Although a temporal interval existed between ICESat-2 data derived in 2019 and in situ data obtained in 2014, a significant correlation was observed between derived bathymetry data and in situ bathymetry data (see Fig. 7). Our results indicate that the coral reef terrain in the study area did not change much from 2014 to 2019, and the ICESat-2 data can be used instead of in situ water depth in some areas with stable terrain.

VI. Conclusion

On the basis of ICESat-2 ATL03 data and multispectral satellite images from GF-1 and WV-2/3, we proposed a PMCGS approach for obtaining bathymetry of large-scale coral reef areas. In this approach, five parametric SDB models in each geomorphic zone of coral reef habitats were constructed, and the combination of optimal parametric models was extrapolated to 11 reefs in Xisha Islands. Results suggested that the optimal models were the multiple ratios regression model for the reef flat, shallow lagoon, and patch reef zones. The binomial models,

including the single-band binomial model and the ratio binomial model, were optimal for the reef slope and deep lagoon. When extrapolating to other reefs in the Xisha Islands, the proposed PMCGS had an RMSE of 0.91 m in the GF-1 image and 0.70–0.88 m in the WV-2/3 image, which performed better than the PM, RF, SVM, and CNN models without geomorphic segmentation.

The PMCGS method efficiently reduced the impact of substrate and water depth heterogeneity on SDB inversion through geomorphic segmentation and has great potential to derive large-scale bathymetry in Indo-Pacific coral reef habitats. Using SDB methods to achieve higher accuracy, factors that affect the inversion accuracy should be considered, such as the tide, sun glint, temporal interval of dataset, and terrain variation. However, the bathymetric accuracy was relatively low on the reef slope owing to the deep water and steep terrain. A study suggested that machine learning models performed well in deep water [48]. Thus, we will try to obtain more training samples and train machine learning models in this zone in future research. Additionally, owing to the irregular geomorphology in Atlantic and Caribbean coral reefs, further validation is required to assess whether our method is applicable to these regions.

REFERENCES

[1] N. A. J. Graham and K. L. Nash, "The importance of structural complexity in coral reef ecosystems," *Coral Reefs*, vol. 32, no. 2, pp. 315–326, Jun. 2013.

[2] R. W. Grigg, "Depth limit for reef building corals in the Au'au channel, SE Hawaii," *Coral Reefs*, vol. 25, no. 1, pp. 77–84, Mar. 2006.

[3] K. M. Morgan, M. A. Moynihan, N. Sanwlani, and A. D. Switzer, "Light limitation and depth-variable sedimentation drives vertical reef compression on turbid coral reefs," *Front. Mar. Sci.*, vol. 7, Nov. 2020, Art. no. 571256.

[4] P. R. Muir, C. C. Wallace, T. Done, and J. D. Aguirre, "Limited scope for latitudinal extension of reef corals," *Science*, vol. 348, no. 6239, pp. 1135–1138, Jun. 2015.

[5] C. Roelfsema et al., "Coral reef habitat mapping: A combination of object-based image analysis and ecological modelling," *Remote Sens. Environ.*, vol. 208, pp. 27–41, Apr. 2018.

[6] M. Zhao et al., "Comparison of coral diversity between big and small atolls: A case study of Yongle atoll and Lingyang reef, Xisha Islands, central of South China Sea," *Biodivers. Conserv.*, vol. 26, no. 5, pp. 1143–1159, May 2017.

[7] X. Zuo, F. Su, H. Zhao, J. Zhang, Q. Wang, and D. Wu, "Regional hard coral distribution within geomorphic and reef flat ecological zones determined by satellite imagery of the Xisha Islands, South China Sea," *Chin. J. Oceanol. Limnol.*, vol. 35, no. 3, pp. 501–514, Jun. 2017.

[8] T. P. Hughes et al., "Coral reefs in the anthropocene," *Nature*, vol. 546, no. 7656, pp. 82–90, Jun. 2017.

[9] M. D. Spalding and B. E. Brown, "Warm-water coral reefs and climate change," *Science*, vol. 350, no. 6262, pp. 769–771, Nov. 2015.

[10] D. Su, F. Yang, Y. Ma, K. Zhang, J. Huang, and M. Wang, "Classification of coral reefs in the South China Sea by combining airborne LiDAR bathymetry bottom waveforms and bathymetric features," *IEEE Trans. Geosci. Remote Sens.*, vol. 57, no. 2, pp. 815–828, Feb. 2019.

[11] J. D. Hedley et al., "Remote sensing of coral reefs for monitoring and management: A review," *Remote Sens*, vol. 8, no. 2, Feb. 2016, Art. no. 118.

[12] M. Ashphaq, P. K. Srivastava, and D. Mitra, "Review of near-shore satellite derived bathymetry: Classification and account of five decades of coastal bathymetry research," *J. Ocean Eng. Sci.*, vol. 6, no. 4, pp. 340–359, Mar. 2021.

[13] A. G. Dekker et al., "Intercomparison of shallow water bathymetry, hydro-optics, and benthos mapping techniques in Australian and Caribbean coastal environments," *Limnol. Oceanogr., Methods*, vol. 9, pp. 396–425, Sep. 2011.

[14] Z. P. Lee, K. L. Carder, C. D. Mobley, R. G. Steward, and J. S. Patch, "Hyperspectral remote sensing for shallow waters. I. A semianalytical model," *Appl. Opt.*, vol. 37, no. 27, pp. 6329–6338, Sep. 1998.

[15] Z. P. Lee, K. L. Carder, C. D. Mobley, R. G. Steward, and J. S. Patch, "Hyperspectral remote sensing for shallow waters: 2. Deriving bottom depths and water properties by optimization," *Appl. Opt.*, vol. 38, no. 18, pp. 3831–3843, Jun. 1999.

[16] D. R. Lyzenga, N. R. Malinas, and F. J. Tanis, "Multispectral bathymetry using a simple physically based algorithm," *IEEE Trans. Geosci. Remote Sens.*, vol. 44, no. 8, pp. 2251–2259, Aug. 2006.

[17] D. R. Lyzenga, "Passive remote sensing techniques for mapping water depth and bottom features," *Appl. Opt.*, vol. 17, no. 3, pp. 379–383, Feb. 1978.

[18] A. Knudby and G. Richardson, "Incorporation of neighborhood information improves performance of SDB models," *Remote Sens. Appl.-Soc. Environ.*, vol. 32, Nov. 2023, Art. no. 101033.

[19] L. Li, "Remote sensing bathymetric inversion for the Xisha Islands based on WorldView-2 data: A case study of Zhaoshu Island and South Island," *Remote Sens. Land Resour.*, vol. 28, no. 4, pp. 170–175, Dec. 2016.

[20] H. Su, H. Liu, L. Wang, A. M. Filippi, W. D. Heyman, and R. A. Beck, "Geographically adaptive inversion model for improving bathymetric retrieval from satellite multispectral imagery," *IEEE Trans. Geosci. Remote Sens.*, vol. 52, no. 1, pp. 465–476, Jan. 2014.

[21] B. Cao et al., "An active-passive fusion strategy and accuracy evaluation for shallow water bathymetry based on ICESat-2 ATLAS laser point cloud and satellite remote sensing imagery," *Int. J. Remote Sens.*, vol. 42, no. 8, pp. 2783–2806, Jun. 2021.

[22] A. Le Quilleuc, A. Collin, M. F. Jasinski, and R. Devillers, "Very high-resolution satellite-derived bathymetry and habitat mapping using Pleiades-1 and ICESat-2," *Remote Sens*, vol. 14, no. 1, Dec. 2022, Art. no. 133.

[23] X. Zhang et al., "Nearshore bathymetry based on ICESat-2 and multispectral images: Comparison between Sentinel-2, Landsat-8, and testing Gaofen-2," *IEEE J. Sel. Topics Appl. Earth Observ. Remote Sens.*, vol. 15, pp. 2449–2462, Feb. 2022.

[24] Y. Ma et al., "Satellite-derived bathymetry using the ICESat-2 lidar and Sentinel-2 imagery datasets," *Remote Sens. Environ.*, vol. 250, Dec. 2020, Art. no. 112047.

[25] N. Xu, X. Ma, Y. Ma, P. Zhao, J. Yang, and X. H. Wang, "Deriving highly accurate shallow water bathymetry from Sentinel-2 and ICESat-2 datasets by a multitemporal stacking method," *IEEE J. Sel. Topics Appl. Earth Observ. Remote Sens.*, vol. 14, pp. 6677–6685, Jun. 2021.

[26] T. Han et al., "Cost-efficient bathymetric mapping method based on massive active-passive remote sensing data," *ISPRS J. Photogramm. Remote Sens.*, vol. 203, pp. 285–300, Sep. 2023.

[27] J. Cheng et al., "A comprehensive evaluation of machine learning and classical approaches for spaceborne active-passive fusion bathymetry of coral reefs," *ISPRS Int. J. Geo-Inf.*, vol. 12, no. 381, Sep. 2023, Art. no. ijgi12090381.

[28] S. Li, X. Wang, Y. Ma, and F. Yang, "Satellite-derived bathymetry with sediment classification using ICESat-2 and multispectral imagery: Case studies in the South China Sea and Australia," *Remote Sens*, vol. 15, no. 4, Feb. 2023, Art. no. 1026.

[29] Y. Liu et al., "Multispectral bathymetry via linear unmixing of the benthic reflectance," *IEEE J. Sel. Topics Appl. Earth Observ. Remote Sens.*, vol. 11, no. 11, pp. 4349–4363, Nov. 2018.

[30] E. C. Geyman and A. C. Maloof, "A simple method for extracting water depth from multispectral satellite imagery in regions of variable bottom type," *Earth Space Sci.*, vol. 6, no. 3, pp. 527–537, Mar. 2019.

[31] R. Ahola, R. Chénier, M. Sagram, and B. Horner, "The impact of sensors for satellite derived bathymetry within the Canadian arctic," *Geomatica*, vol. 74, no. 2, pp. 46–64, Jun. 2020.

[32] P. Wicaksono, S. D. Harahap, and R. Hendriana, "Satellite-derived bathymetry from WorldView-2 based on linear and machine learning regression in the optically complex shallow water of the coral reef ecosystem of Kemujan island," *Remote Sens. Appl.-Soc. Environ.*, vol. 33, Nov. 2024, Art. no. 101085.

[33] C. Cahalane, A. Magee, X. Monteys, G. Casal, J. Hanafin, and P. Harris, "A comparison of Landsat 8, RapidEye and Pleiades products for improving empirical predictions of satellite-derived bathymetry," *Remote Sens. Environ.*, vol. 233, Nov. 2019, Art. no. 111414.

[34] S. R. Phinn, C. M. Roelfsema, and P. J. Mumby, "Multi-scale, object-based image analysis for mapping geomorphic and ecological zones on coral reefs," *Int. J. Remote Sens.*, vol. 33, no. 12, pp. 3768–3797, Dec. 2012.

[35] R. P. Stumpf, K. Holderied, and M. Sinclair, "Determination of water depth with high-resolution satellite imagery over variable bottom types," *Limnol. Oceanogr.*, vol. 48, no. 1, part 2, pp. 547–556, Jan. 2003.
[36] M. A. Huston and M. A. Huston, *Biological Diversity: The Coexistence of Species*. Cambridge, U.K., MA, USA: Cambridge Univ. Press, 1994.
[37] C. E. Parrish, L. A. Magruder, A. L. Neuenschwander, N. Forfinski-Sarkozi, M. Alonzo, and M. Jasinski, "Validation of ICESat-2 ATLAS bathymetry and analysis of ATLAS's bathymetric mapping performance," *Remote Sens*, vol. 11, no. 14, Jul. 2019, Art. no. 4303.
[38] F. Sun, W. Sun, J. Chen, and P. Gong, "Comparison and improvement of methods for identifying waterbodies in remotely sensed imagery," *Int. J. Remote Sens.*, vol. 33, no. 21, pp. 6854–6875, Nov. 2012.
[39] J. Hedley, A. Harborne, and P. Mumby, "Simple and robust removal of sun glint for mapping shallow-water benthos," *Int. J. Remote Sens.*, vol. 26, no. 10, pp. 2107–2112, May 2005.
[40] A. Albright and C. Glennie, "Nearshore bathymetry from fusion of Sentinel-2 and ICESat-2 observations," *IEEE Geosci. Remote Sens. Lett.*, vol. 18, no. 5, pp. 900–904, May 2021.
[41] C. Xie, P. Chen, D. Pan, C. Zhong, and Z. Zhang, "Improved filtering of ICESat-2 lidar data for nearshore bathymetry estimation using Sentinel-2 imagery," *Remote Sens.*, vol. 13, no. 21, Oct. 2021, Art. no. 4303.
[42] G. Zheng, F. Chen, and Y. Shen, "Detecting the water depth of the South China Sea reef area from WorldView-2 satellite imagery," *Earth Sci. Informat.*, vol. 10, no. 3, pp. 331–337, Sep. 2017.
[43] J. D. Hedley et al., "Coral reef applications of Sentinel-2: Coverage, characteristics, bathymetry and benthic mapping with comparison to Landsat 8," *Remote Sens. Environ.*, vol. 216, pp. 598–614, Oct. 2018.
[44] M. Liceaga-Correa and J. Euan-Avila, "Assessment of coral reef bathymetric mapping using visible Landsat Thematic Mapper data," *Int. J. Remote Sens.*, vol. 23, no. 1, pp. 3–14, Nov. 2002.
[45] F. Dang and Q. Ding, "A technique for extracting water depth information from multispectral scanner data in the South China Sea," *Mar. Sci. Bull.*, vol. 22, no. 3, pp. 55–60, Jun. 2003.
[46] Y. Wang, Y. Chen, X. Zhou, L. Yang, and Y. Fu, "Research on reef bathymetry using remote sensing based on polynomial regression model," *Acta Oceanol. Sin.*, vol. 40, no. 3, pp. 121–128, Mar. 2018.
[47] Y. Le et al., "Investigating the shallow-water bathymetric capability of Zhuhai-1 spaceborne hyperspectral images based on ICESat-2 data and empirical approaches: A case study in the South China Sea," *Remote Sens.*, vol. 14, no. 14, Jul. 2022, Art. no. 3406.
[48] C. Liu et al., "Accurate refraction correction—Assisted bathymetric inversion using ICESat-2 and multispectral data," *Remote Sens*, vol. 13, no. 21, Oct. 2021, Art. no. 4355.
[49] W. N. Zhou et al., "A comparison of machine learning and empirical approaches for deriving bathymetry from multispectral imagery," *Remote Sens.*, vol. 15, no. 2, Jan. 2023, Art. no. 393.
[50] M. Ashphaq, P. K. Srivastava, and D. Mitra, "Satellite-derived bathymetry in dynamic coastal geomorphological environments through machine learning algorithms," *Earth Space Sci.*, vol. 11, Jul. 2024, Art. no. e2024EA003554.
[51] X. Zuo, F. Su, H. Zhao, Y. Fang, and J. Yang, "Development of a geomorphic classification scheme for coral reefs in the South China Sea based on high-resolution satellite images," *Prog. Geog.*, vol. 37, no. 11, pp. 1463–1472, Nov. 2018.
[52] S. Andréfouët and M. Paul, "Atolls of the world: A reappraisal from an optical remote sensing and global mapping perspective," *Mar. Pollut. Bull.*, vol. 194, Aug. 2023, Art. no. 115400.
[53] M. B. Lyons et al., "New global area estimates for coral reefs from high-resolution mapping," *Cell Rep. Sustain.*, vol. 1, Feb. 2024, Art. no. 100015.
[54] B. Chen, Y. Yang, and K. Luo, "Retrieval of island shallow water depth from the GaoFen-1 multispectral imagery," *J. Trop. Oceanogr.*, vol. 36, no. 2, pp. 70–78, Nov. 2017.
[55] J. Liang, J. Zhang, and Y. Ma, "A spatial resolution effect analysis of remote sensing bathymetry," *Acta Oceanol. Sin.*, vol. 36, pp. 102–109, Jul. 2017.
[56] H. J. Hsu et al., "A semi-empirical scheme for bathymetric mapping in shallow water by ICESat-2 and Sentinel-2: A case study in the South China Sea," *ISPRS J. Photogramm. Remote Sens.*, vol. 178, pp. 1–19, Aug. 2021.
[57] X. Zhang, Y. Ma, J. Zhang, and J. Cheng, "Research on the remote sensing inversion fusion model of shallow water depth based on the piecewise adaptive algorithm," *Mar. Sci.*, vol. 44, no. 6, pp. 1–11, Feb. 2020.
[58] H. Guo, H. Yang, B. Qiao, M. Wang, and L. Zhu, "Multi-resolution satellite images bathymetry inversion of Bangda Co in the western Tibetan Plateau," *Int. J. Remote Sens.*, vol. 42, no. 21, pp. 8077–8098, Nov. 2021.

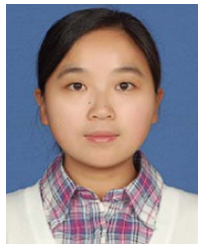

Xiuling Zuo received the Ph.D. degree in cartography and geographic information system from the Institute of Geographic Sciences and Natural Resources Research, Chinese Academy of Sciences, Beijing, China, in 2016.

She is currently an Associate Professor with the Guangxi University, Nanning, China. Her current research interest includes remote sensing of coral reef resources and environment.

Juncan Teng received the B.S. degree in marine science in 2021 from the Guangxi University, Nanning, China, where he is currently working toward the Ph.D. degree in biology.

His current research interest includes remote sensing and ecology of coral reefs.

Fenzhen Su received the Ph.D. degree in cartography and geographic information system from Institute of Geographic Sciences and Natural Resources Research, Chinese Academy of Sciences, Beijing, China, in 2001.

He is currently a Professor with the institute of Geographic Sciences and Natural Resources Research, Chinese Academy of Sciences. His current research interest includes coastal remote sensing, geographic information systems, and high-dimensional spatio-temporal Big Data intelligence.

Zhengxian Duan received the M.S. degree in marine science from the Guangxi University, Nanning, China, in 2022.

His current research interest includes remote sensing and geographic information system of coral reefs.

Kefu Yu received the Ph.D. degree in geochemistry from Guangzhou Institute of Geochemistry, Chinese Academy of Sciences, Guangzhou, China, in 2000.

He is currently a Professor with the Guangxi University, Nanning, China, and an Adjunct Scientist with the Southern Marine Science and Engineering Guangdong Laboratory (Guangzhou), Guangzhou, China. His current research interest includes geology, ecology, and environment of coral reefs.